JACS
JOURNAL OF THE AMERICAN CHEMICAL SOCIETY

ARTICLE

pubs.acs.org/JACS

Ultra-fast Rotors for Molecular Machines and Functional Materials via Halogen Bonding: Crystals of 1,4-Bis(iodoethynyl)bicyclo[2.2.2]octane with Distinct Gigahertz Rotation at Two Sites

Cyprien Lemouchi,[†] Cortnie S. Vogelsberg,[‡] Leokadiya Zorina,[†,§] Sergey Simonov,[†,§] Patrick Batail,[*,†] Stuart Brown,[*,∥] and Miguel A. Garcia-Garibay[*,‡]

[†]Laboratoire MOLTECH-Anjou, Université d'Angers, CNRS, 2 Boulevard Lavoisier, 49045 Angers, France

[‡]Department of Chemistry, University of California—Los Angeles, 607 Charles E. Young Drive East, Los Angeles, California 90095-1569, United States

[§]Institute of Solid State Physics, Russian Academy of Sciences, Chernogolovka, 142432 MD, Russia

[∥]Department of Physics, University of California—Los Angeles, Box 951547, Los Angeles, California 90095-1569, United States

Supporting Information

ABSTRACT: As a point of entry to investigate the potential of halogen-bonding interactions in the construction of functional materials and crystalline molecular machines, samples of 1,4-bis-(iodoethynyl)bicyclo[2.2.2]octane (BIBCO) were synthesized and crystallized. Knowing that halogen-bonding interactions are common between electron-rich acetylenic carbons and electron-deficient iodines, it was expected that the BIBCO rotors would be an ideal platform to investigate the formation of a crystalline array of molecular rotors. Variable temperature single crystal X-ray crystallography established the presence of a halogen-bonded network, characterized by lamellarly ordered layers of crystallographically unique BIBCO rotors, which undergo a reversible monoclinic-to-triclinic phase transition at 110 K. In order to elucidate the rotational frequencies and the activation parameters of the BIBCO molecular rotors, variable-temperature ^{1}H wide-line and ^{13}C cross-polarization/magic-angle spinning solid-state NMR experiments were performed at temperatures between 27 and 290 K. Analysis of the ^{1}H spin−lattice relaxation and second moment as a function of temperature revealed two dynamic processes simultaneously present over the entire temperature range studied, with temperature-dependent rotational rates of $k_{rot} = 5.21 \times 10^{10}\ s^{-1} \cdot \exp(-1.48\ kcal \cdot mol^{-1}/RT)$ and $k_{rot} = 8.00 \times 10^{10}\ s^{-1} \cdot \exp(-2.75\ kcal \cdot mol^{-1}/RT)$. Impressively, these correspond to room temperature rotational rates of 4.3 and 0.8 GHz, respectively. Notably, the high-temperature plastic crystalline phase I of bicyclo[2.2.2]octane has a reported activation energy of 1.84 kcal·mol^{-1} for rotation about the 1,4 axis, which is 24% larger than $E_a = 1.48$ kcal·mol^{-1} for the same rotational motion of the fastest BIBCO rotor; yet, the BIBCO rotor has three fewer degrees of translational freedom and two fewer degrees of rotational freedom! Even more so, these rates represent some of the fastest engineered molecular machines, to date. The results of this study highlight the potential of halogen bonding as a valuable construction tool for the design and the synthesis of amphidynamic artificial molecular machines and suggest the potential of modulating properties that depend on the dielectric behavior of crystalline media.

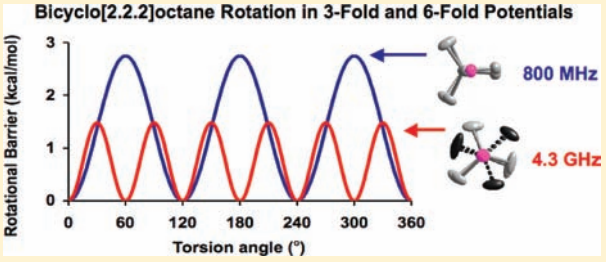

INTRODUCTION

The field of artificial molecular machines represents one of the most interesting challenges in basic science and modern technology.[1,2] While there has been much progress made in the design of sophisticated small molecule analogs of macroscopic machines,[1,2] one of the most promising perspectives is based on the realization that complex molecular-level properties and functions can be manifested in a collective manner at the macroscopic scale in the form of complex functional materials.[3,4] With materials applications in mind, one of the greatest challenges is the need to develop crystal engineering strategies to control not only the number of components and their organization but also their internal dynamics. In the past few years, our research groups in Angers and in Los Angeles have been working on the development of multicomponent crystalline conductors[5−7] and the design of amphidynamic crystals with rapidly moving parts.[8−10] Now, we have joined forces to explore systems where the dielectric modulation inherent to the rotor dynamics[11,12] may affect the electrostatic potential of a charge carriers' environment, which is expected to cause transitions between conducting and localized states.[5,13] Although this is a subject of much current interest that has been stimulated by sound theories,[14,15] it has been only approached experimentally by

Received: January 18, 2011
Published: April 06, 2011

   dx.doi.org/10.1021/ja200503j | J. Am. Chem. Soc. 2011, 133, 6371–6379

analysis of charge-transfer processes and hole migration affected by collective hydrogen-bond activation[16] and dynamics.[17] As a starting point to engineer functional crystals modulated by ultrafast molecular rotors, we propose to take advantage of strategies based on halogen-bonding interactions.[18] The latter has been used for the design of multicomponent crystalline conductors[5,19] and appears to be significantly robust. Halogen bonds occur between electron-deficient halogens and electron-rich atoms with interaction energies that vary between ca. 1−43 kcal/mol, depending on the electron density of the donor.[20,21] To transition into molecular rotors, we set out to analyze the use of halogen bonding as a lattice-directing interaction to control the organization of a rotor array.[8−10] It has been shown that molecular structures inspired by macroscopic gyroscopes with high-symmetry rotators[22] linked by triple bonds to bulky stator groups facilitate internal rotation in the crystalline state (Scheme 1a). For this study we selected bis(1,4-iodoethynyl) bicyclo[2.2.2]octane (BIBCO) as a promising test case. Based on a previous report with the analogous 1,4-bis(iodoethynyl) benzene,[5,23] we recognized that iodine atoms covalently linked to each terminal acetylenic carbon would provide the elements required for a halogen-bonded network through iodine—acetylene interactions at the two ends of each rotator, as shown in Scheme 1b.[24,25] The C_3-symmetric bicyclo[2.2.2]octane rotator was selected knowing that cylindrically shaped, higher-order C_n rotators, with $n > 2$, pack in a manner that does not generate high rotational barriers.[22]

As described in detail below, the desired packing arrangement was obtained according to expectations. Extensive X-ray diffraction experiments and structure analysis as a function of temperature demonstrated that crystals of BIBCO undergo a disorder−order phase transition at 110 K from monoclinic ($C2/c$) to triclinic ($P\bar{1}$) structures, with rotational disorder in the high-temperature phase. To measure the rotational dynamics of the cylindrical bicyclo[2.2.2]octane rotator, and expecting frequencies in the megahertz (MHz) regime at ambient temperature, we decided to use ^{1}H NMR spin−lattice relaxation (T_1) as a function of temperature. Spin−lattice relaxation can be used to probe dynamic processes occurring at frequencies that are near the Larmor frequency of the nucleus being studied: ^{1}H at 26.4 and 300 MHz in our experiments. In addition, spin−lattice relaxation is particularly useful when the stimulated nuclear transitions responsible for restoring thermal equilibrium in the sample are determined by the modulation of dipolar interactions caused by the rapid motion of internal rotors.[26] The fastest relaxation (a minimum in T_1) occurs at the temperature when the rotator matches the Larmor frequency. In the case of BIBCO crystals, analysis of the ^{1}H spin−lattice relaxation between 27 and 290 K revealed two T_1 minima, indicating that there are two distinct but simultaneous rotational processes over the entire temperature range. This observation is in general agreement with crystal structure, where BIBCO molecules are in two different sites with different environments.

Scheme 1

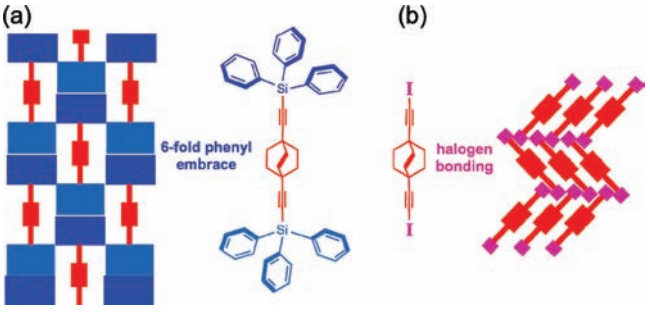

RESULTS AND DISCUSSION

Sample Preparation. Samples of bis(1,4-iodoethynyl)bicyclo-[2.2.2]octane (BIBCO) were obtained in 76% yield by iodination of 1,4-diethynylbicyclo[2.2.2]octane (BCO) **9** with *N*-iodosuccinimide (NIS). The terminal dialkyne was synthesized from diethylsuccinate in a nine-step sequence developed in Angers using diverse literature procedures, as illustrated in Scheme 2, with an overall yield of 11%. The modified synthesis is analyzed in detail in the Supporting Information Section along with all the spectroscopic and analytical data. Colorless, diamond-shaped single crystals of BIBCO were obtained by recrystallization from hot ethanol.

X-ray Structures Determination at 295, 130, and 90 K. Single crystal X-ray diffraction data was collected on a Bruker Nonius KappaCCD diffractometer [λ(Mo K$_\alpha$) = 0.71073 Å] equipped with an Oxford Cryosystems cryostream cooler. Unit cell parameters were measured in the temperature range of 295−90 K with 5−30° steps (Figure SI-1, Supporting Information). A reversible phase transition from a monoclinic $C2/c$ to a triclinic $P\bar{1}$ structure was identified upon cooling below 110 K. Full X-ray data sets were collected at 295, 130, and 90 K by a combined φ- and ω-scan method. The triclinic structure is twinned; diffraction intensities from both twin domains were integrated into SHELX HKLF5 file using the EVALCCD software.[27] Analytical absorption corrections were applied for the 90 K data using WINGX,[28]

Scheme 2. Nine Step Sequence of BCO[a]

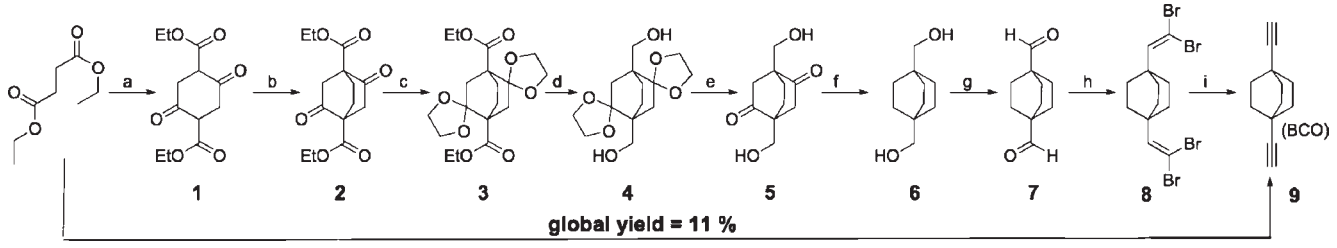

[a] Reagents for each step include: (a) NaH, dimethoxyethane, 60 °C, 15 h, 78% yield; (b) NaH, 1,2-dibromoethane, 110 °C, 96 h, 85% yield; (c) *p*-TsOH, diethyleneglycol, toluene, reflux, 48h, 71% yield; (d) $LiAlH_4$, Et_2O, reflux, 5 h, 93% yield; (e) HCl 0.1 M, reflux, 24 h, quant.; (f) KOH, hydrazine monohydrate, diethyleneglycol, reflux, 48 h, 41% yield; (g) Oxalylchloride, DMSO, CH_2Cl_2, Et_3N, quant.; (h) CBr_4, PPh_3, CH_2Cl_2, R.T, 5 h, 65% yield; and (i) *n*-BuLi (2.5 M), THF, −78 °C, 1 h, 95% yield. (See Supporting Information).

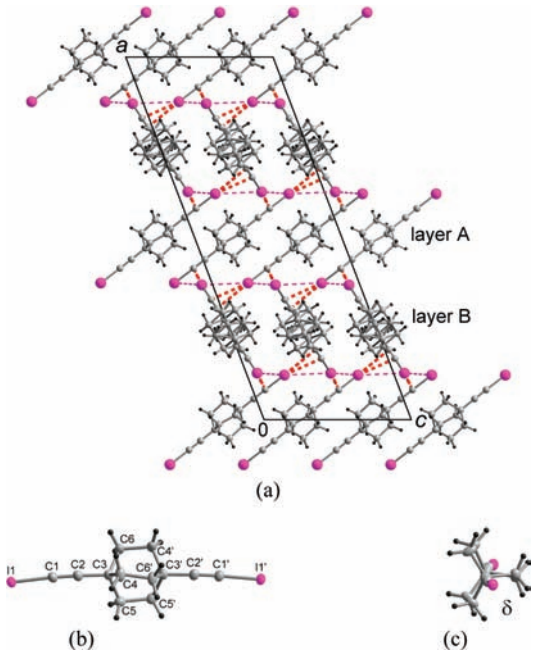

Figure 1. The high-temperature, monoclinic BIBCO structure. (a) Structure projection along the *b* axis of unit cell. Layer A: layer of molecules A with one equilibrium position; and layer B: layer of molecules B with two equilibrium positions. The structure is directed by a set of C−I···π shown here in dashed red lines (I···C distances at 130 K are 3.330(3) and 3.469(3) Å (I_A···C_B) and 3.425(3) Å (I_B···C_A); C−I, 1.991(3) and 1.994(3) Å) and C−I···I−C halogen bonds drawn in dashed purple lines (I···I, 3.9483(3) and 4.0028(4) Å). (b) The BIBCO rotor axles in layer A are slightly bent. (c) While the rotator is chiral as a result of a helical twist, the centrosymmetric crystal contains a racemic mixture of the δ and λ conformers.

while empirical multiscan absorption correction with SADABS[29] was used for the 295 and 130 K data. The structures were solved by a direct method followed by Fourier syntheses and refined by a full-matrix least-squares method in an anisotropic approximation for all nonhydrogen atoms using the SHELX-97 programs.[30] Hydrogen (H)-atoms in the bicyclo[2.2.2]octane fragments were introduced in calculated positions with U_{iso}(H) = 1.2 U_{eq}(C). Table S1, Supporting Information summarizes the main crystal and refinement data.

Solid-State ^{13}C CP/MAS NMR. The ^{13}C cross-polarization/magic-angle spinning (CP/MAS) spectra of a finely powdered crystalline BIBCO sample, acquired at UCLA on a Bruker Avance 300 solid-state spectrometer operating at a ^{13}C frequency of 75 MHz, displayed three sharp signals at δ 102.50, 32.68, 29.14 ppm, corresponding to the inner acetylenic C(sp), methylene C(sp^3), and bridge head C(sp^3), respectively. These are similar to the ^{13}C signals at 100.70, 31.43, 28.40 ppm, respectively, observed in a CD_2Cl_2 solution at 125 MHz. It is of interest to note the signal corresponding to the acetylenic C(sp) bonded to the iodine appears as a weak, broad signal at 0.79 ppm in the solid state (Figure SI-2, Supporting Information) yet appears at −6.35 ppm in a CD_2Cl_2 solution (Figure SI-3, Supporting Information).[31] This is an indication that the solid-state shielding effects of iodine may be due, to a significant extent, to C−I···I−C halogen-bonding interactions. In agreement with previous studies, MAS failed to completely remove the dipolar coupling between the spin-1/2 ^{13}C nucleus and the quadrupolar spin-5/2 ^{127}I nucleus, thus resulting in the observed signal broadening.[32]

VT ^{1}H Spin−Lattice Relaxation (T_1). To determine the rotational dynamics and activation energy of the molecular rotors in BIBCO, spin−lattice relaxation (T_1) measurements were carried out at UCLA at two different ^{1}H Larmor frequencies (300 and 26.4 MHz) and over a wide range of temperatures in the solid state. Wide-line ^{1}H spectra from 27 to 220 K were measured in single crystals with a commercial electromagnet using a NMR spectrometer and probe built at UCLA. The typical NMR frequency used was 26.4 MHz with the electromagnet set to a field strength B_0 of 0.6225 T. A very small NMR coil was constructed using bare copper wire wound on a wire form. A few single crystals were loaded into the coil at random orientations and held in place with a Teflon tube and caps. Acetone was used for cleaning the coil and its surroundings to reduce spurious proton signals relative to the BIBCO sample. ^{1}H spin−lattice relaxation was measured using a saturation recovery sequence combined with a spin−echo in which a saturation pulse comb (3 * $\pi/2$) was followed a time τ' later (τ' values taken from the variable delay list) with a $\pi/2$ pulse p_1 (typical pulse width p_1 = 1.3 μs) and subsequently a pulse p_2. The angle of p_2 is adjustable to maximize the spin−echo magnitude, and pulses were calibrated at different temperatures as necessary. Saturation recovery traces from 220 to 50 K were fit well with a single exponential function (Figure SI-4, Supporting Information). Data traces below 50 K began to deviate from a monoexponential. Measurements between 189 to 290 K were performed on a polycrystalline BIBCO sample and acquired with a Bruker Avance 300 solid-state NMR spectrometer. ^{1}H spin−lattice relaxation was measured via the inversion−recovery method using ^{13}C CP/MAS detection. The ^{13}C CP/MAS spectra were acquired at a ^{13}C frequency of 75 MHz and a ^{1}H frequency of 300 MHz. Details regarding the experimental parameters of spectra acquisition may be found in the Supporting Information. At each temperature between 189 to 290 K, the data was fit well with a monoexponential function (Figure SI-5, Supporting Information).

Halogen Bonding as Crystal Engineering Strategy. The crystal structure at ambient temperature was solved in the monoclinic space group *C*2/*c* with eight molecules per unit cell. A view of the structure along *b* in Figure 1a illustrates a layered topology where two independent slabs, A and B, alternate along *a*. The layers differ by the type of packing as well as the positional ordering of the bicyclo-[2.2.2]octane rotators. Each layer contains one crystallographically independent BIBCO molecule. Molecules in layer A lie on a two-fold monoclinic axis and are fully ordered. Molecules in layer B are located on inversion centers, and their acentric inner bicyclo[2.2.2]octane rotator fragment is disordered between two distinct equilibrium positions of equal weights. In order to investigate the fate of the disorder for molecules B as a function of temperature, the structure was studied in a wide temperature range. A series of unit cell parameters measured between 295 and 90 K revealed a monoclinic to triclinic structural phase transition at 110 K identified by the appearance of additional weak Bragg reflections. Full X-ray diffraction data were collected at 295, 130, and 90 K. As the crystal structures at room temperature and 130 K are almost identical, a detailed comparative analysis of the monoclinic structure at 130 K and the triclinic one at 90 K, above and below the phase transition temperature, is presented below.

As shown in Figure 1b, the rotor axle is not linear, but it is instead slightly bent toward one of the three bicyclo[2.2.2]octane rotor blades. Another salient feature is the axial chirality of the bicyclo[2.2.2]octane rotator, with a C_3 point group that originates from a common tilt of the three rotator blades. However, the crystal contains a racemic mixture of the right (δ in Figure 1c) and left (λ) conformers, as required by the centrosymmetric space group.[33] The BIBCO molecules from adjacent layers are orthogonal to each other in such a way that C−I···π intermolecular interactions shown by red dashed lines in Figure 1a and C−I···I−C halogen bonds are both satisfied. The I atoms of the ordered A molecule form two similar short I···C contacts to both C atoms of the triple C≡C bond of the molecule in the other layer, 3.330(3) and 3.469(3) Å for (I_A···C_B) at 130 K. In contrast, one of two (I_B···C_A) contacts from I atoms of the disordered B molecule is much shorter than the other: 3.425(3) and 3.666(3) Å.

dx.doi.org/10.1021/ja200503j |*J. Am. Chem. Soc.* 2011, 133, 6371–6379

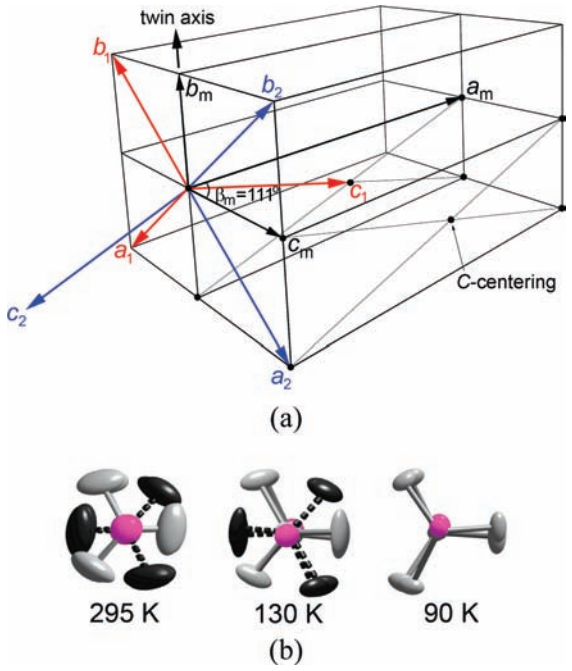

Figure 2. (a) Lattice transformation at the monoclinic to triclinic phase transition. Monoclinic cell vectors are drawn in black, while two triclinic lattices, 1 and 2, are marked by red and blue colors, respectively. The *a* and *b* axes of the new triclinic lattice go along the diagonal directions of *bc* monoclinic layer (i.e., the lattice periodicity becomes twice in both b_m and c_m directions), while the new *c*-axis corresponds to C-centering vector of the monoclinic C-lattice (see unit cell parameters in Table S1, Supporting Information). Twin lattices 1 and 2 are related by a 180° rotation around the b_m-axis, which was the monoclinic axis in the original monoclinic cell. The refined twin fraction is 0.4685(5). (b) Positional ordering upon the transition. As temperature is decreased from 295 to 130 K, the anisotropic displacement parameters of the rotor atoms become smaller. At 90 K, only one equilibrium position remains.

These C−I···π intermolecular interactions can be seen as a particular case of directional halogen bonding where the electron-depleted polar regions of the polarized iodine atoms reach out toward the electron-rich p_π orbitals of primarily one or eventually two carbon atoms of the triple bond. Though an early example of this interaction was documented in tetragonal crystalline diiodoacetylene (C_2I_2),[24] this type of halogen bond has been largely overlooked.[21,25] A more recent example comes from our earlier analysis of the crystal structure of 1,4-bis(iodoethynyl)benzene (Figure SI-6, Supporting Information), which is similar to that of BIBCO. We also note that a loose, single C_{sp3}−I···I halogen interaction is identified in the layered structure of 1,4-diiodobicyclo[2.2.2]octane (Figure SI-7, Supporting Information).[34]

Cooling the crystal below 110 K reveals additional Bragg reflections associated with a phase transition from the monoclinic *C*2/*c* to a twinned triclinic $P\bar{1}$ structure. Note that the orthogonality between the monoclinic *b*-axis and the *ac*-plane is not affected and that the lattice distortion upon the transition is minimal (Figure SI-1, Supporting Information). However, the pattern of systematic diffraction absences as well as structural ordering resulting from the transition could only be correctly described in a triclinic lattice twinned by a two-fold rotation around the former monoclinic axis (Figure 2a). The most important structural changes in the low-temperature phase concern the rotators in layer B (Figure 2b). Specifically, they lose local inversion symmetry and become ordered below the phase transition. As shown in Figure 2b, the bicyclo[2.2.2]octane atoms in the *C*2/*c* structure at 295 K display large anisotropic displacement parameters for

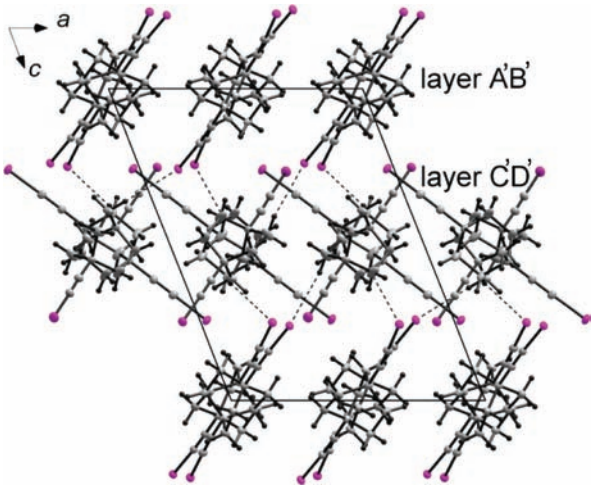

Figure 3. Triclinic crystal structure at 90 K (drawn with 50% ellipsoid probability). The set of shortest C−H···I hydrogen bonds with $H_{C',D'}\cdots I_{B',A'}$ = 3.04−3.11 Å is shown by dashed lines.

the two rotator orientations, pointing to two relatively shallow minima for the two equilibrium populations that are dynamically averaged out over time during the X-ray data collection. At 130 K, the positional disorder remains, but the anisotropic displacements parameters are smaller, as expected for a smaller librational displacement. Finally, at 90 K, only one equilibrium position remains, indicating that one of the two sites becomes substantially lower in energy in the new $P\bar{1}$ crystal phase. Relevant, striking changes in experimental electron density maps are shown in Figure SI-8, Supporting Information.

The low-temperature triclinic structure is shown projected along *b* in Figure 3. Below the transition, each layer consists of two independent molecules in general positions, each with only one equilibria position. Layers A′B′ and C′D′ in the $P\bar{1}$ crystal phase, respectively, correspond to layers A and B of the *C*2/*c* structure shown in Figure 1a. Note that the crystal remains achiral across the phase transition since the triclinic structure is also centrosymmetric.

The patterns of intermolecular interactions inside layers A′B′ and C′D′ are different (Figure 4). The rotor axles within layer A′B′ are close to parallel. In contrast, the axles of molecules C′ and D′ are orthogonal. As a result, rotors from the A′B′ and C′D′ layers have fundamentally different molecular environments (see also Figures SI-9 and 10, Supporting Information). Both layers consist of segregated rows of the alternating, inversionally related δ and λ molecules of the same name: ···A′A′A′··· and ···B′B′B′··· rows run along *b* in layer A′B′ (Figure 4a), while ···C′C′C′··· and ···D′D′D′··· rows are parallel to [$\bar{1}$10] in layer C′D′ (Figure 4b). The motif linking the ethynyl stator fragments via C−I···π and C−I···I−C interactions remains intact across the transition, although the contact distances change in a way (see Figure SI-10 and Table S2, Supporting Information for a comparison of contact distances at different temperatures). The intermolecular interaction between rotors and stator fragments occurs by hydrogen bonding with I atoms as acceptors. The shortest C−H···I bonds (dashed lines in Figure 3) involve iodine atoms of molecules A′ and B′ and −CH_2 groups of formerly disordered molecules C′ and D′ ($H_{C'}\cdots I_{B',A'}$ = 3.07 and 3.09 Å; $H_{D'}\cdots I_{A',B'}$ = 3.04 and 3.11 Å). These are likely to interfere in the process of ordering the C′ and D′ rotors. For a comparison, other similar contacts of the $H_{A',B'}\cdots I_{C',D}$, $H_{A',B'}\cdots I_{A',B'}$, and $H_{C',D'}\cdots I_{C',D'}$ types both between and inside the layers exceed 3.25, 3.27, and 3.24 Å, respectively.

Effects of Molecular and Crystal Symmetries on Rotational Potentials. While crystals of BIBCO have two crystallographically independent molecules above the phase transition and four below, the

dx.doi.org/10.1021/ja200503j |*J. Am. Chem. Soc.* 2011, 133, 6371–6379

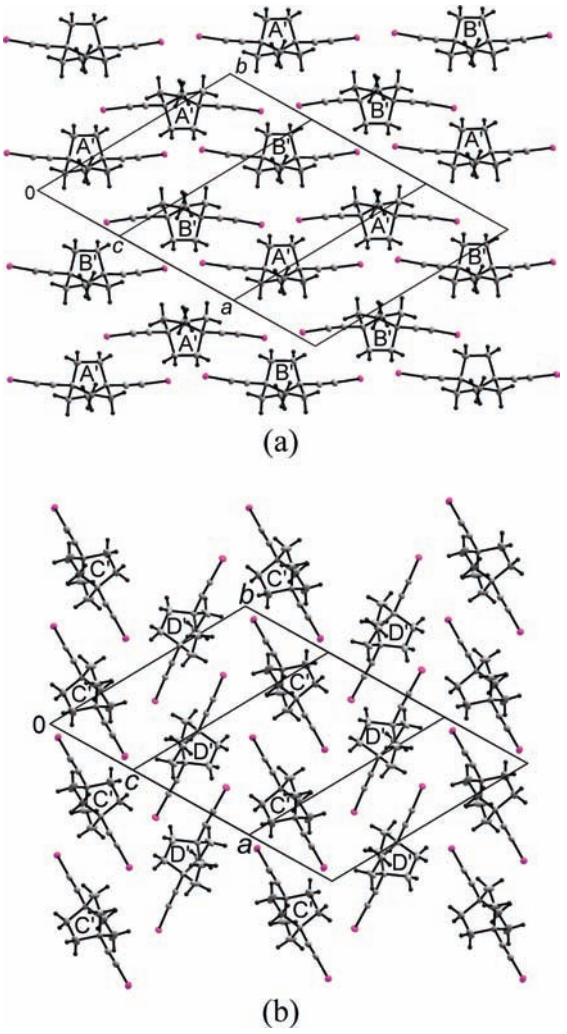

Figure 4. These projections of the A′B′ layer (a) and C′D′ layer (b) along c^* exemplify the difference in molecular arrangement.

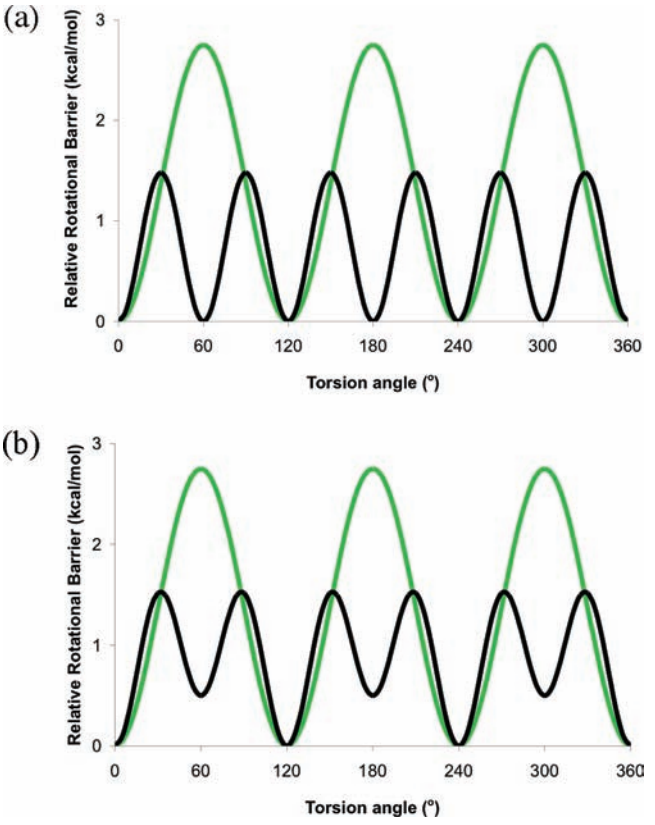

Figure 5. (a) Proposed high-temperature rotational potential for the ordered layer A (green) and disordered layer B (black) layers. (b) Proposed low-temperature rotational potential for the ordered three-fold layer A (green) and the formally ordered six-fold layer B (black) rotators. Each layer has two crystallographically distinct molecules, but each pair has a very similar environment.

two forms are essentially congruent. The local interactions remain relatively unaltered at the disorder−order phase transition. Although it could have been expected that the spin−lattice relaxation in the BIBCO crystal might have required double and triple exponential functions to fit the kinetics of crystallographically independent rotors, relaxation was monoexponential over a wide temperature range, suggesting a system under magnetic equilibrium and with a common spin temperature. However, two energy minima in the ^{1}H T_1 versus temperature plot (vide infra) clearly indicate that relaxation is determined by two kinetically distinct rotational processes, which contribute equally to the T_1 relaxation of the crystal. Based on these observations, our NMR analysis will rely on the assumption that the steric environment of the rotator can be described in terms of two types rotors located in the two different layers, A (A′B′ when T < 110 K) and B (C′D′ when T < 110 K), over the entire temperature range investigated. In layer A, the bicyclo[2.2.2]octane rotators are always ordered with a local three-fold symmetry characterized by jumps that occur via 120° displacements and a barrier of 2.75 kcal·mol^{-1} (vide infra). The potential assigned to this site at high temperature is shown in green in Figure 5a. In layer B, the bicyclo[2.2.2]octane rotators are positionally disordered at high temperatures and, by symmetry, have a six-fold rotational potential with six isoenergetic minima that have equal populations. The barrier of this site is 1.48 kcal·mol^{-1}, and the potential assigned to this site is shown in black in Figure 5a.

When cooling a BIBCO crystal to lower temperatures, the disorder of molecules in the B layer lessens and then gradually disappears (Figure 2b). Below the phase transition at 110 K, the inversion center on molecule B is absent, and all molecules are ordered. The rotational potential of the originally ordered, three-fold symmetric site of rotators in the high-temperature A layer (A′B′ layer at T < 110 K) remains essentially unchanged (shown in green), but the potential of the six-fold symmetric site of rotators in the high-temperature B layer (C′D′ layer at T < 110 K) is no longer isoenergetic with respect to the six sites. The molecules at low temperature have a preferred orientation that correspond to three low-energy minima, but the other three minima are maintained, though slightly higher in energy, as shown in black in Figure 5b. The crystal structure reveals the population corresponding to the preferentially occupied sites, but rotational dynamics are likely to occur in 60° jumps. The residence time in the higher energy sites should be shorter, and their equilibrium populations smaller (note that a difference of ca. 0.5 kcal·mol^{-1} between the high- and low-energy minima would result in equilibrium populations of ca. 94:6 at T = 90 K, which would be difficult to detect crystallographically).

VT ^{1}H Spin−Lattice relaxation (T_1). The equilibration of magnetic nuclei in condensed phases occurs by stimulated transitions that result from the local magnetic fields generated by dynamic processes of nearby spins in the lattice. It is well-known that spin−lattice relaxation in solid samples may be dominated by a particular dynamic process if some portions of the lattice are fairly static while others experience rapid motion. When a single process with a correlation time τ_c is responsible for the T_1 relaxation, it is possible to determine the parameters that

dx.doi.org/10.1021/ja200503j |J. Am. Chem. Soc. 2011, 133, 6371–6379

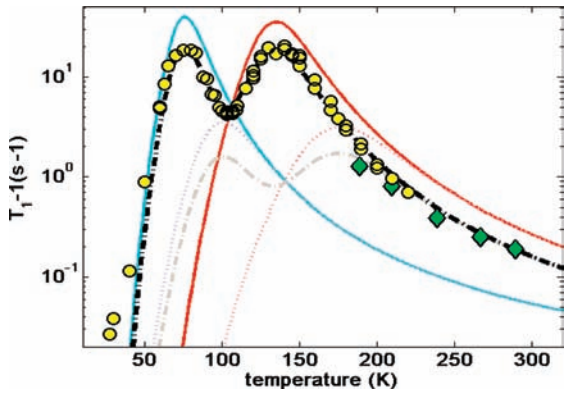

Figure 6. Temperature dependence of the ^{1}H spin−lattice relaxation time (T_1) in BIBCO displaying two T_1^{-1} maxima observed at 26.4 MHz (yellow circles) and 300 MHz (green tilted squares). The heavy blue and red lines correspond to a Kubo−Tomita fit for the two processes at 26.4 MHz, assuming Arrhenius-type behavior. The dotted black line corresponds to the weighted sum of these two processes observed at 26.4 MHz and displays an excellent fit to the data. The light-blue and light-red dotted lines correspond to a Kubo−Tomita fit for the two processes at 300 MHz, assuming Arrhenius-type behavior. The dotted gray line corresponds to the weighted sum of these two processes observed at 300 MHz.

characterize its potential by measuring the T_1 as a function of temperature. Specifically, if a motional process responsible for relaxation has a correlation time τ_c equal to the inverse Larmor frequency of the observed nucleus, then the relaxation will be most efficient and a minimum in the spin−lattice relaxation time will be observed.[26] Consequently, the activation energy E_a for a thermally activated process having a τ_c with Arrhenius-type temperature dependence (eq 1) may be derived by fitting the T_1 data to the Kubo−Tomita eq 2:

$$\tau_c = \tau_0 \exp(E_a/kT) \quad (1)$$

$$T_1^{-1} = C[\tau_c(1+\omega_0^2\tau_c^2)^{-1} + 4\tau_c(1+4\omega_0^2\tau_c^2)^{-1}] \quad (2)$$

where the constant $C = (2/3)\ \gamma^2\,\mathbf{B}_{nuc}^2$ corresponds to the dipolar interactions related to the relative positions of the nuclei that participate in the relaxation. $\mathbf{B}_{nuc}$ is the local effective dipolar field, and γ and ω_0 are the gyromagnetic ratio and the angular Larmor precession frequency, respectively, of the observed nucleus in a magnetic field.[35]

From the spin−lattice relaxation (T_1) measurements performed between 27 and 290 K, a logarithmic plot of T_1^{-1} as a function of temperature displayed an excellent agreement with the ^{1}H T_1 measurements acquired by the inversion−recovery method at 300 MHz (Figure 6, green diamonds) and by the saturation recovery method at 26.4 MHz (yellow circles). Interestingly, the plot revealed two T_1^{-1} maxima, suggesting that spin−lattice relaxation occurs by two distinct motional processes with dominant contributions at different temperatures. At 26.4 MHz, a low-energy process resonates with the ^{1}H Larmor frequency at ca. 80 K, resulting in a T_1 minimum of 53 ms. A second, higher energy process reaches the frequency of 26.4 MHz at ca. 130 K and results in another T_1 minimum of 51 ms. No discontinuity in T_1 values was observed at the phase transition determined by X-ray diffraction at 110 K, confirming that the transition arises from minor structural changes that affect the symmetry of the unit cell without affecting the sterics and dynamics of the bicyclo[2.2.2]octane rotators. Temperature cycling around the phase transition revealed no hysteresis in T_1^{-1}, again consistent with the X-ray crystallographic studies, further suggesting that the two polymorphs are an enantiotropic pair.[36] We conclude that the position of the minimum in the relaxation rate (T_1^{-1}) versus temperature plot, also at ca. 110 K in Figure 6, is coincidental. While the variable-temperature data at 300 MHz is limited, the full range of the T_1^{-1} data estimated with the Kubo−Tomita equation at 26.4 MHz versus 300 MHz (vide infra) accounts for the small divergence between green tilted squares and yellow circles below 200K, as expected for a change in the position of the inflection point for the two T_1^{-1} maxima at the two different spectrometer frequencies.

VT ^{1}H T_1 Data Analysis. Recognizing that the structures of the two BIBCO polymorphs are closely related and that both arrange in alternating lamellarly ordered layers of rotators with different packing motifs, we interpret the two T_1^{-1} maxima as corresponding to the rotational motion of the bicyclo[2.2.2]octane rotators about their 1,4-axis in the two different crystallographic layers A and B. The low-energy rotational process is associated with the less sterically hindered layer B, which displays rotational disorder in both of the high-temperature crystal structures obtained at 295 and 130 K, while the higher energy process is associated with rotation in the more sterically hindered, ordered layer A. This assignment is supported by the fact that the shortest T_1 relaxation times for each process are essentially equivalent (53 ms versus 51 ms), suggesting that they do arise from two different processes with effectively equal dipolar averaging but different frequencies. Assuming that the reorientation of the BIBCO rotators in each environment provides the dominant spin−lattice relaxation and that the protons exist at a common spin-temperature within the lattice, the T_1 behavior observed for the system may be expressed as the weighted sum of the two distinct rotational processes:[37]

$$T_1^{-1}{}_{total} = (0.5)T_1^{-1}{}_{fast} + (0.5)T_1^{-1}{}_{slow} \quad (3)$$

where the weighting factors (0.5) are related to the total fraction of different nuclei responsible for motional averaging of the dipolar interactions within the unit cell. The component $T_{1\ fast}$ is the temperature-dependent spin−lattice relaxation for the low-energy rotational process from rotators in layer B, and $T_{1\ slow}$ is the temperature-dependent spin−lattice relaxation for the higher energy process for rotators in layer A. The total number of molecules is the same in the different layers. Therefore, each layer and its associated motional process contribute equally to the total spin−lattice relaxation observed over the entire temperature range studied.

To elucidate the activation energy and attempt frequency for BIBCO dynamics, each individual rotational process from the T_1 data was subjected to a Kubo−Tomita fit by applying eq 2 and assuming an Arrhenius-type temperature dependence for the corresponding correlation times, $\tau_{c\ fast}$ and $\tau_{c\ slow}$. The corresponding variations shown as a relaxation rate, or T_1^{-1}, as a function of temperature are illustrated in red and blue lines in Figure 6. Adding the two processes together with the corresponding weighting factors (eq 3) gave an excellent match with the observed experimental data when the Arrhenius equation values, τ_o and E_a, were optimized for the fast and slow components (Figure 6, black dotted line). Notably, the sum of the two processes is required to obtain a good fit at higher temperatures, helping dismiss the possibility that the low-barrier process is present only in the low-temperature polymorph. From the constant C of the Kubo−Tomita equation, the magnitude of the local effective dipolar field $\mathbf{B}_{nuc} = -[\gamma h\mu_0/(4\pi R^3)](1 - 3\cos^2\theta)\boldsymbol{m}_1$, where R is internuclear distance, can be found. This value was extracted from the fit of the experimental T_1^{-1} versus temperature data and found to be ca. 3 gauss (G). This value is consistent with the magnitude $\mathbf{B}_{nuc} = [\gamma h\mu_0/(4\pi R^3)]$ calculated from the interhydrogen distances in the BIBCO structure, where $R \geq 2.70$ Å corresponding to a $\mathbf{B}_{nuc}$ magnitude of 2.7 G and lower for protons on adjacent carbons.

The low-energy process with a T_1^{-1} maximum at ca. 80 K was fit to an activation energy of 1.48 kcal·mol^{-1} and a pre-exponential factor (or attempt frequency) $A = 5.21 \times 10^{10}$ s^{-1}.[38] The higher energy process, with a T_1 minimum at ca. 130 K, has an activation energy of 2.75 kcal·mol^{-1} and an attempt frequency of $A = 8.00 \times 10^{10}$ s^{-1}.[39] The activation energies of the rotators in the two different layers are

dx.doi.org/10.1021/ja200503j |J. Am. Chem. Soc. 2011, 133, 6371–6379

Table 1. Arrhenius and Eyring Parameters Derived from a Kubo−Tomita Fit of the T_1 Data

	E_a (kcal·mol^{-1})	$\Delta H^{\ddagger}$ (kcal·mol^{-1})	A (s^{-1})	τ_0 (s)	$\Delta S^{\ddagger}$ (cal/K·mol)
disordered layer	1.48	1.48	5.21×10^{10}	1.92×10^{-11}	2.50
ordered layer	2.75	2.47	8.00×10^{10}	1.25×10^{-11}	−0.45

consistent with the crystallographic data, which indicates two crystallographically distinct environments with different steric barriers. The activation parameters indicate that rotators in the disordered layer have a frequency of ca. 4.3 GHz at ambient temperature, while the corresponding frequency for the ordered layer is ca. 0.8 GHz. Comparatively, in the high-temperature plastic crystalline phase I, pure bicyclo[2.2.2]octane has an activation energy of 1.84 kcal·mol^{-1} for rotation about the 1,4 axis.[40] This is 24% larger than E_a = 1.48 kcal·mol^{-1} for the same rotational motion about the 1,4-axis of bicyclo[2.2.2]octane in the faster BIBCO rotor. Yet, the BIBCO rotor has two fewer degrees of rotational freedom!

Activation Parameters. Given that the two (three- and six-fold) BIBCO rotators in the separate layers A and B have the same moment of inertia and intrinsic (gas phase) molecular electronic barrier, a comparison of their activation parameters is particularly interesting. Assigning the high and low barriers to the ordered and disordered three- and six-fold potentials, respectively, is consistent with the crystallographic data and the two local BIBCO environments. Furthermore, differences in the two pre-exponential factors (A_{fast} and A_{slow}) are experimentally significant. Specifically, the BIBCO rotators in the six-fold, low E_a layer possess an attempt frequency that is ca. 35% smaller than that of the ordered BIBCO rotators with the higher barrier. Given that the attempt frequency represents the highest jumping frequency for the thermally activated rotator in a particular environment, it is significant that rotators in the two layers possess different rotational symmetry orders and different potentials. According to transition-state theory, the attempt frequency is related to the frequency of the librational mode that describes the oscillation of the rotator, ν_{Lib}, which is determined by the shape of the potential. To gain a qualitative insight, we assume a simple symmetric rotational potential with n-energy minima and a barrier E_{max} as a function of the angle Θ, as described by a cosine function of the form:

$$E(\Theta) = 1/2E_{max}[1 - \cos n\Theta] \quad (4)$$

The frequency of the active librational mode, ν_{Lib}, will depend on the shape of the function as determined by E_{max} and n. Steeper potentials will result the higher the librational frequencies and greater the pre-exponential factors. Steeper potentials will arise from higher barriers and, for a given barrier height, from a greater number of minima. In the case of BIBCO, a barrier of E_a = 2.75 kcal·mol^{-1} for the ordered three-fold symmetric layers is almost twice as large as that for the disordered layers with the six-fold energy minima, which has an E_a = 1.48 kcal·mol^{-1}. Using these values in eq 4 demonstrates that the depth and shape of the potentials are very similar, suggesting that the corresponding librational modes should have analogous frequencies and that the different attempt frequencies result from the additional vibrational activation required to reach the top of the barrier.

A potentially important limitation of the Arrhenius analysis is that it assumes the pre-exponential factor is constant over the entire temperature range studied. To account for such variations one may apply the Eyring eq 5:

$$\tau_c = h/k_B T \exp(-\Delta S^{\ddagger}/R) \exp(\Delta H^{\ddagger}/RT) \quad (5)$$

to substitute the τ_c in the Kubo−Tomita expression (Figure SI-12, Supporting Information). An excellent fit to the T_1^{-1} data was obtained with a $\Delta H^{\ddagger}$ = 1.48 kcal·mol^{-1}and $\Delta S^{\ddagger}$ = 2.50 cal/K·mol for the low-energy, six-fold rotary process and with $\Delta H^{\ddagger}$ = 2.47 kcal·mol^{-1}and $\Delta S^{\ddagger}$ = −0.45 cal/K·mol for the higher energy, three-fold rotary process. The $\Delta H^{\ddagger}$ values are in excellent agreement with the E_a obtained from the Arrhenius analysis, and the activation entropies are very small, and nearly zero, for both the six- and three-fold rotators, respectively (Table 1). The relatively small activation entropy for a single rotation step may be interpreted as an indication that no correlated motion or changes in order is required, and a small and positive value for the disordered layers may reflect the "dissociative" nature of the lower energy potential.

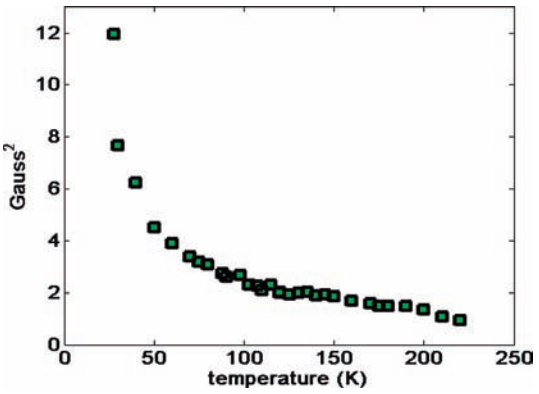

Figure 7. The ^{1}H NMR second moment as a function of temperature.

Second Moment Analysis (M_2). The proton second moment (M_2) is the mean square width of the proton wide-line curve and hence is related to the spin−spin relaxation (T_2).[26] Like the spin−lattice relaxation, both M_2 and T_2 are modulated by dipolar interactions, which are averaged in the presence of molecular motion. While static molecules in the solid-state display very broad signals, molecules undergoing fast reorientation display narrowed signals. The ^{1}H M_2 for BIBCO was measured as a function of temperature from 27 to 220 K at 26.4 MHz (Figure 7). No distinguishable plateaus were observed, thus indicating that BIBCO motion changes continuously throughout the entire temperature range investigated. At 220 K, M_2 is 0.97 G^2. Cooling to 50 K resulted in observable line broadening, resulting in an increased M_2 value of 4.5 G^2. There is no discontinuity in M_2 at the phase transition at 110 K, supporting the notion that there are no significant structural changes that affect the dynamics of the rotators. Further cooling from 50 to 27 K resulted in a rapid increase in M_2 up to 12 G^2, indicating an abrupt decrease in molecular rotation. Although temperatures below 27 K were not explored due to limitations of the NMR probe setup, the data suggest that further line broadening would occur below 27 K, up to the limit of the rigid lattice when BIBCO rotation is frozen or at the limit of quantum mechanical tunneling if rotations may occur from zero point energy levels.

In order to qualitatively evaluate line-broadening effects as a function of temperature, the motionally narrowed line width at 220 K was related to the correlation time of the BIBCO rotors in the disordered layer B and the magnitude of the local effective field $\mathbf{B}_{nuc}$ determined from the Kubo−Tomita fit. In the high-temperature limit, when $\omega_0^2 \tau_c^2 \ll 1$:

$$\text{mean } ^1\text{H linewidth}_{\text{high}T} \approx T_2^{-1}{}_{\text{high}T} \approx T_1^{-1}{}_{\text{high}T} \approx (2/3)\gamma^2 \mathbf{B}_{nuc}{}^2 \tau_{c,\text{fast}} \quad (6)$$

At T = 220 K, the mean width of the motionally narrowed ^{1}H wide-line spectrum is at a minimum of ca. 4.1 kHz. According to the above eq 6,

dx.doi.org/10.1021/ja200503j |J. Am. Chem. Soc. 2011, 133, 6371–6379

line-broadening effects due to a decrease in the rotational dynamics should become relevant when the fastest rotator layer becomes sufficiently slow to cease partial averaging of dipolar interactions, i.e., when the averaged dipolar interactions become the same order of magnitude as the motionally narrowed line width. Using the narrowed line width at T = 220 K, eq 6 reveals this temperature to be approximately 70 K. Consistent with the results of this calculation, the ^{1}H M_2 data reveal a dramatic increase in spectral line width below 70 K. Above this temperature, the rotational correlation time becomes very small, and the rotational processes sufficiently fast, leading to a partial averaging of dipolar interactions. This result confirms the validity of the Kubo−Tomita fit and relates the dynamic rotational processes affecting ^{1}H M_2 to the averaged internuclear ^{1}H dipolar fields of the BIBCO rotors.

CONCLUSIONS

In order to investigate the potential of halogen bonding for the design and the synthesis of functional materials and molecular machines, a halogen-bonded network of BIBCO molecular rotors was synthesized and structurally characterized using single crystal X-ray diffraction data from 295 to 90 K. The structural solution revealed a halogen-bonded, lamellar structure composed of alternating ordered (A) and disordered (B) layers of BIBCO rotors in two crystallographically unique environments, which undergo a disorder−order phase transition at 110 K. The Brownian rotational dynamics of the crystallographically distinct bicyclo[2.2.2]octane rotators in the two layers were each assigned a distinct, clearly resolved dynamic process due to the relaxation contribution from each kinetically distinguishable A and B site based upon variable-temperature solid-state NMR studies from 290 to 27 K. Remarkably, the rotational dynamics of both layers are ultra-fast at room temperature, with frequencies corresponding to 0.8 and 4.3 GHz, respectively. The activation energy for rotation about the 1,4-bicyclo[2.2.2]octane axis is 24% lower in the disordered B layer of BIBCO, as compared to the high-temperature plastic crystalline phase I of the bicyclo-[2.2.2]octane molecule. This study validates an unprecedented approach to the construction of amphidynamic molecular machines where the extended framework itself provides the template to differentiate rotor dynamics and to sustain engineered rotation down to very low temperatures. With respect to the frequency factors of the BIBCO rotators in the ordered and disordered layers, analysis of the data suggests that different rotational potentials and solid-state packing dictate the limiting rotational dynamics, even though the rotors possess the same intrinsic electronic (gas phase) barrier. Although spin−lattice relaxation measurements cannot discern the type of rotational motion present, analysis of the crystal structure suggests that rotational symmetry order of three- and six-fold symmetries may play an important role on the dynamics of the two distinguishable rotators. Future studies involving deuterium-enriched BIBCO rotors may help elucidate the jumping mechanism of the two layers using variable-temperature quadrupolar echo ^{2}H NMR. The results of this study confirm that halogen bonding is a valuable tool for the construction of functional materials and artificial molecular machines.

ASSOCIATED CONTENT

Supporting Information. Sample ^{1}H wide-line and ^{13}C CP/MAS spectra, T_1 relaxation curves, solid-state ATR-FT/IR, synthetic information, additional crystallographic information, and a Kubo−Tomita fit using the Eyring analysis. This material is available free of charge via the Internet at http://pubs.acs.org.

AUTHOR INFORMATION

Corresponding Author

mgg@chem.ucla.edu; Patrick.Batail@univ-angers.fr; brown@physics.ucla.edu.

ACKNOWLEDGMENT

We thank the National Science Foundation for support through grants DMR-0605688 (MGG), 0804625 (SB), and DGE-0654431 IGERT: Materials Creation Training Program (CSV) as well as the California NanoSystems Institute (CSV). We thank the CNRS and the Région des Pays de la Loire for support through a joint Ph.D. grant (C.L.), an associated CNRS researcher position (L.Z.), a PDL Post-Doctorate grant (S.S.), and grant MOVAMOL-2010 10306.

REFERENCES

(1) (a) van Delden, R. A.; Wiel, M. K. J.; Pollard, M. M.; Vicario, J.; Koumura, N.; Feringa, B. L. *Nature* **2005**, *437*, 1337. (b) Horinek, D.; Michl, J. *Proc. Natl. Acad. Sci. U.S.A.* **2005**, *102*, 14175. (c) Skopek, K.; Gladysz, J. A. J. *Organomet. Chem.* **2008**, *693*, 857. (d) Karim, A. R.; Linden, A.; Baldridge, K. K.; Siegel, J. S. *Chem. Sci.* **2010**, *1*, 102. (e) Scarso, A.; Onagi, H.; Rebek, J., Jr. *J. Am. Chem. Soc.* **2004**, *126*, 12728. (f) Leigh, D. A.; Wong, J. K. Y.; Dehez, F.; Zerbetto, F. *Nature* **2003**, *424*, 174. (g) Pease, A. R.; Jeppesen, J. O.; Stoddart, J. F.; Luo, Y.; Collier, C. O.; Heath, J. R. *Acc. Chem. Res.* **2001**, *34*, 433. (h) Jian, H.; Tour, J. M. *J. Org. Chem.* **2003**, *68*, 5091. (i) Akutagawa, T.; Shitagami, K.; Nishihara, S.; Takeda, S.; Hasegawa, T.; Nakamura, T.; Hosokoshi, Y.; Inoue, K.; Ikeuchi, S.; Miyazaki, Y.; Saito, K. *J. Am. Chem. Soc.* **2005**, *127*, 4397.

(2) (a) Kay, E. R.; Leigh, D. A.; Zerbetto, F. *Angew. Chem., Int. Ed.* **2007**, *46*, 72. (b) Skopek, K.; Hershberger, M. C.; Gladysz, J. A. *Coord. Chem. Rev.* **2007**, *251*, 1723. (c) Browne, W. R.; Feringa, B. L. *Nat. Nanotechnol.* **2006**, *1*, 25. (d) Kottas, G. S.; Clarke, L. I.; Horinek, D.; Michl, J. *Chem. Rev.* **2005**, *105*, 1281.

(3) (a) Garcia-Garibay, M. A. *Angew Chem. Int. Ed.* **2007**, *46*, 8945. (b) Garcia-Garibay, M. A. *Nat. Mater.* **2008**, *7*, 431.

(4) (a) Akutagawa, T.; Endo, D.; Kudo, F.; Noro, S.-I.; Takeda, S.; Cronin, L.; Nakamura, T. *Crys. Growth Design* **2008**, *8*, 812. (b) Akutagawa, T.; Sato, D.; Koshinaka, H.; Aonuma, M.; Noro, S.-I.; Takeda, S.; Nakamura, T. *Inorg. Chem.* **2008**, *47*, 5951. (c) Akutagawa, T.; Nakamura, T. *Dalton Trans.* **2008**, *45*, 6335. (d) Kitagawa, H.; Kobori, Y.; Yamanaka, M.; Yoza, K.; Kobayashi, K. *Proc. Nat. Acad. Sci. U. S.A.* **2009**, *106*, 10444.

(5) A recent example involves conducting crystals of [EDT-TTF]$_8$-[1,4-bis(iodoethynyl)benzene] [$Re_6Se_8(CN)_6$] (EDT-TTF is ethylenedithio-tetrathiafulvalene), with alternating single layers of EDT-TFF and single hybrid slabs directed by halogen bonds between the polarized, electrophilic iodine atoms of 1,4-bis(iodoethynyl)benzene (*p*-BiB) and the Lewis basic cyanide groups of the anionic octahedral hexanuclear rhenium complex $Re_6Se_8(CN)_6$: Barrès, A.-L.; El-Ghayoury, A.; Zorina, L.; Canadell, E.; Auban-Senzier, P.; Batail, P. *Chem. Commun.* **2008**, 2194.

(6) (a) Chow, D. S.; Zamborszky, E.; Alavi, B.; Tantillo, D. J.; Baur, A.; Merlic, C. A.; Brown, S. E. *Phys. Rev. Lett.* **2000**, *85*, 1698. (b) Zamborzky, F.; Yu, W.; Rass, W.; Brown, S. E.; Alavi, B.; Merlic, C. A.; Baur, A. *Phys. Rev. B* **2002**, *66*, 081103. (c) Auban-Senzier, P.; Pasquier, C. R.; Jérome, D.; Suh, S.; Brown, S. E.; Mézière, C.; Batail, P. *Phys. Rev. Lett.* **2009**, *102*, 257001.

(7) It has been shown that hydrogen-bonding dynamics are coupled to Mott localization at metal-to-insulator transitions that set upon charge ordering and Wigner crystallization: Zorina, L.; Simonov, S.; Mézière,

C.; Canadell, E.; Suh, S.; Brown, S. E.; Foury-Leylekian, P.; Fertey, P.; Pouget, J.-P.; Batail, P. *J. Mater. Chem.* **2009**, *19*, 6980.

(8) (a) Khuong, T. V.; Zepeda, G.; Ruiz, R.; Khan, S. I.; Garcia-Garibay, M. A. *Cryst. Growth Des.* **2004**, *4*, 15. (b) Godinez, C. E.; Zepeda, G.; Mortko, C. J.; Dang, H.; Garcia-Garibay, M. A. *J. Org. Chem.* **2004**, *69*, 1652. (c) Karlen, S. D.; Ortiz, R. O.; Chapman, O. L.; Garcia-Garibay, M. A. *J. Am. Chem. Soc.* **2005**, *127*, 6554. (d) Nunez, J. E.; Natarajan, A.; Khan, S. I.; Garcia-Garibay, M. A. *Org. Lett.* **2007**, *9*, 3559. (e) Godinez, C. E.; Garcia-Garibay, M. A. *Cryst. Growth Des.* **2009**, *9*, 3124.

(9) (a) Horansky, R. D.; Clarke, L. I.; Price, J. C.; Khuong, T.-A. V.; Jarowski, P. D.; Garcia-Garibay, M. A. *Phys. Rev. B.* **2005**, *B72*, 014302. (b) Rodriguez-Molina, B.; Ochoa, E. M.; Farfán, N.; Santillan, R.; Garcia-Garibay, M. A. *J. Org. Chem.* **2009**, *74* (22), 8554.

(10) (a) Karlen, S.; Khan, S. I.; Garcia-Garibay, M. A. *Cryst. Growth Des.* **2005**, *5*, 53. (b) Dominguez, Z.; Dang, H.; Strouse, M. J.; Garcia-Garibay, M. A. *J. Am. Chem. Soc.* **2001**, *124*, 2398. (c) Dominguez, Z.; Khuong, T.-A. V.; Dang, H.; Sanrame, C. N.; Nunez, J. E.; Garcia-Garibay, M. A. *J. Am. Chem. Soc.* **2003**, *125*, 8827. (d) Dominguez, Z.; Dang, H.; Strouse, M. J.; Garcia-Garibay, M. A. *J. Am. Chem. Soc.* **2002**, *124*, 7719.

(11) Horinek, D.; Michl, J. *Proc. Nat. Acad. Sc.* **2005**, *102*, 14175.

(12) Akutagawa, T.; Koshinaka, H.; Sato, D.; Takeda, S.; Noro, S.-I.; Takahashi, H.; Kumai, R.; Tokura, Y.; Nakamura, T. *Nat. Mater.* **2009**, *8*, 342.

(13) Miyagawa, K.; Kanoda, K.; Kawamoto, A. *Chem. Rev.* **2004**, *104*, 5635.

(14) Seo, H.; Hotta, C.; Fukuyama, H. *Chem. Rev.* **2004**, *104*, 5005.

(15) Giamarchi, T. *Chem. Rev.* **2004**, *104*, 5037.

(16) (a) García, P.; Dahaoui, S.; Katan, C.; Souhassou, M.; Lecomte, C. *Faraday Discuss.* **2007**, *135*, 217. (b) Baudron, S. A.; Batail, P.; Rovira, C.; Canadell, E.; Clérac, R. *Chem. Commun.* **2003**, 1820. (c) Baudron, S. A.; Avarvari, N.; Canadell, E.; Auban-Senzier, P.; Batail, P. *Chem.—Eur. J.* **2004**, *10*, 4498.

(17) (a) Akutagawa, T.; Saito, G.; Yamochi, Y.; Kusunoki, M.; Sakaguchi, K. *Synth. Met.* **1995**, *69*, 591. (b) Itoh, T.; Kitagawa, H.; Mitani, T.; Nakasuji, K. *Chem. Lett.* **1995**, 41. (c) Murata, T.; Morita, Y.; Yakiyama, Y.; Fukui, K.; Yamochi, H.; Saito, G.; Nakasuji, K. *J. Am. Chem. Soc.* **2007**, *129*, 10837. (d) Wu, J. C.; Dupont, N.; Liu, S.-X.; Neels, A.; Hauser, A.; Decurtins, S. *Chem. Asian J.* **2009**, *4*, 392. (e) Yuasa, J.; Yamada, S.; Fukuzumi, S. *J. Am. Chem. Soc.* **2008**, *130*, 5808. (f) Mohammed, O. F.; Kwon, O.-H.; Othon, C. M.; Zewail, A. H. *Angew. Chem., Int. Ed.* **2009**, *48*, 6251. (g) El-Ghayoury, A.; Mézière, C.; Simonov, S.; Zorina, L.; Cobián, M.; Canadell, E.; Rovira, C.; Náfrádi, B.; Sipos, B.; Forró, L.; Batail, P. *Chem.—Eur. J.* **2010**, *16*, 14051.

(18) (a) Metrangolo, P.; Meyer, F.; Pilati, T.; Resnati, G.; Terraneo, G. *Angew. Chem., Int. Ed.* **2008**, *47*, 6114. (b) Rissanen, K. *CrystEngComm* **2008**, *10*, 1107. (c) Derossi, S.; Brammer, L.; Hunter, C. A.; Ward, M. D. *Inorg. Chem.* **2009**, *48*, 1666. (d) Sarwar, M. G.; Dragisic, B.; Salsberg, L. J.; Gouliaras, C.; Taylor, M. S. *J. Am. Chem. Soc.* **2010**, *132*, 1646. (e) Metrangolo, P.; Resnati, G. *Science* **2008**, *321*, 918. (f) Fourmigué, M.; Batail, P. *Chem. Rev.* **2004**, *104*, 5379. (g) Fourmigué, M. *Struct. Bonding (Berlin)* **2008**, *126*, 181. (h) Metrangolo, P.; Pilati, T.; Terraneo, G.; Biella, S.; Resnati, G. *CrystEngComm* **2009**, *11*, 1187. (i) Kilah, N. L.; Wise, M. D.; Serpell, C. J.; Thompson, A. L.; White, N. G.; Christensen, K. E.; Paul D. Beer, P. D. *J. Am. Chem. Soc.* **2010**, *132*, 11893.

(19) (a) Yamamoto, H. M.; Yamaura, J.-I.; Kato, R. *J. Am. Chem. Soc.* **1998**, *120*, 5905. (b) Kosaka, H.; Yamamoto, H. M.; Nakao, A.; Kato, R. *Bull. Chem. Soc. Jpn.* **2006**, *79*, 1148.

(20) (a) Metrangolo, M.; Resnati, G.; Pilati, T.; Liantonio, R.; Meyer, F. *J. Polym. Sci., Part A: Polym. Chem.* **2007**, *45*, 1. (b) Raatikainen, K.; Rissanen, K. *Cryst. Eng. Comm.* **2009**, *11*, 750. (c) Lu, Y.; Shi, T.; Wang, Y.; Yang, H.; Yan, X.; Luo, X.; Jiang, H.; Zhu, W. *J. Med. Chem.* **2009**, *52*, 2854.

(21) Crystal engineering with I···I and C−I···π halogen bonds: (a) Muniappan, S.; Lipstman, S.; Goldberg, I. *Chem. Commun.* **2008**, 1777. (b) Lipstman, S.; Muniappan, S.; Goldberg, I. *Cryst. Growth Des.* **2008**, *8*, 1682.

(22) Karlen, S. D.; Reyes, H.; Taylor, R. E.; Khan, S. I.; Hawthorne, M. F.; Garcia-Garibay, M. A. *Proc. Natl. Acad. Sci. U.S.A.* **2010**, *107*, 14973.

(23) Kosaka, Y.; Yamamoto, H. M.; Nakao, A.; Kato, R. *Bull. Chem. Soc. Jpn.* **2006**, *79*, 1148.

(24) (a) Dunitz, J. D.; Gehrer, H.; Britton, D. *Acta Cryst. B* **1972**, *28*, 1989. (b) Ghassemzadeh, M.; Harms, K.; Denicke, K. *Chem. Ber.* **1996**, *129*, 259.

(25) Adams, C. J. L.; Bowen, E. *Dalton Trans.* **2005**, 2239.

(26) Fyfe, C. A. *Solid State NMR for Chemists*; C.F.C. Press: Guelph, Ontario, 1983.

(27) Duisenberg, A. J. M.; Kroon-Batenburg, L.; Schreurs, A. M. M. *J. Appl. Crystallogr.* **2003**, *36*, 220.

(28) Farrugia, L. J. *J. Appl. Crystallogr.* **1999**, *32*, 837.

(29) Sheldrick, G. M. *SADABS*; University of Göttingen: Göttingen, Germany, 1996.

(30) Sheldrick, G. M. *Acta Crystallogr.* **2008**, *A64*, 112.

(31) The ^{13}C NMR resonances of various acetylenic C(sp)'s bonded to iodides, measured in solution, are typically found between 7 to −12 ppm. Hein, Jason E.; Tripp, Jonathan C.; Krasnova, Larissa B.; Sharpless, K. Barry; Fokin, Valery V. *Angew. Chem. Int. Ed.* **2009**, *48*, 8018.

(32) (a) Zumbulyadis, N.; Henrichs, P. M.; Young, R. H. *J. Chem. Phys.* **1981**, *75*, 1603. (b) Aliev, A. E.; Harris, K. D. M.; Barrie, P. J.; S Camus, S. *J. Chem. Soc. Faraday Trans.* **1994**, *90*, 3729.

(33) It has been shown that the enantiomerization barrier for bicyclo[2.2.2]octane is very low. See (a) Ermer, O.; Dunitz, J. D. *Helv. Chim. Acta* **1969**, *52*, 1861. (b) Yokozeki, A.; Kuchitsu, K.; Morino, Y. *Bull. Chem. Soc. Jpn.* **1970**, *43*, 2017.

(34) Britton, D. *Acta Crystallogr.* **1974**, *B30*, 1304.

(35) (a) Kubo, R.; Tomita, K. *Phys. Soc. Jpn.* **1954**, *9*, 888. (b) Redfield, A. G. *Adv. Magn. Reson.* **1965**, *1*, 1.

(36) Bernstein, J. *Polymorphism in Molecular Crystals*; Clarendon Press: Oxford, Great Britain, 2002.

(37) (a) Tritt-Goc, J.; Pislewski, N.; Pawlowski, A.; Goc, R. *Solid State Commun.* **1998**, *6*, 367. (b) Medycki, W.; Pislewski, N.; Jakubas, R. *Solid State Nucl. Magn. Reson.* **1993**, *2*, 197. (c) Woessner, J. *Chem. Phys.* **1962**, *36*, 1. (d) Ishida, H.; Ikeda, R.; Nakamura, D. *J. Phys. Chem.* **1982**, *86*, 1003.

(38) This corresponds to a τ_0 of 1.92×10^{-11} s.

(39) This corresponds to a τ_0 of 1.25×10^{-11} s

(40) McGuigan, S.; Strange, J. H.; Chezeau, J. M.; Nasr, M. *J. Phys. (Paris)* **1985**, *46*, 271.